Adsorption characteristics of methylene blue onto low-cost dried and calcined water hyacinth: A batch and fixed-bed column study

Nakorn Suriyanon [1*], Pattra Wongpankamol [1] Siraprapa Chainetr[1] and Wanida Suriyanon[1]
[1] Department of Civil and Environmental Engineering, Faculty of Engineering, Rajamangala University of Technology Lanna, Chiangmai 50300, Thailand
[*]Corresponding Author: jamecu555@gmail.com Phone Number: 089-756-5410
Received: 23 November 2023, Revised: 23 May 2024, Accepted: 29 May 2024

Abstract
This study investigated the potential of using two types of water hyacinth as adsorbents for removing Methylene Blue (MB) from aqueous solutions. The Langmuir isotherm model best fits the adsorption isotherm data, with Dried Water Hyacinth (DWH) performing better than Calcined Water Hyacinth (CWH). The modeling data breakthrough curve indicated that DWH and CWH followed pseudo-second-order kinetics monolayer chemical sorption. Even though DWH has a lower adsorption capacity than activated carbon and other expensive adsorbents, it is comparable to, or performed better than other low-cost adsorbents.
Keywords: Adsorption, Methylene blue, Water hyacinth, Low-cost adsorbent, Fixed bed column

1. Introduction

Synthetic dyes are used in various industries to color products such as textiles, plastics, and leather. However, many of these dyes remain unconsumed and are discharged into effluent, which poses an ecological threat. Dye fixation during the dyeing process depends on the type of dye used. The presence of dyes in effluents reduces light penetration, which affects the metabolic activities of aquatic organisms, thereby threatening aquatic ecosystems and human health. Methylene blue (MB), a cationic dye used in the textile industry, can impair photosynthesis as well as cause skin irritation, cancer, nausea, vomiting, diarrhea, gastritis, eye burning, and mutagenicity in animals. Treatment of MB dye before discharge into freshwater ecosystems is essential.

Various methods are used for treating colored wastewater, including reverse osmosis, sedimentation, ultrafiltration, solvent extraction, adsorption, catalysis, coagulation, ion exchange, and photo-oxidation. Adsorption is a cost-effective way to remove dyes from water [1-2]. Various adsorbents have been studied for removing dyes, metals, pharmaceutical residues, and toxic substances from water [3-4]. Activated carbon is commonly used due to its high adsorption capacity, but it's expensive. Low-cost materials such as kudzu, coir pith, and sawdust are being explored. Many adsorbents, including activated carbon, clay, and nanomaterials, are used for removing MB from water [5-6]. Water hyacinth is a free-floating aquatic plant that can remove pollutants from water. This study uses water hyacinth as an adsorbent to remove MB from water.

2. Materials and methods

2.1 Preparation of adsorbents

Water hyacinths were collected from a public pond in the Mae Rim district, Chiang Mai province. After washing them with tap water, the shoots were sun-dried and oven-dried at 100°C for 24 hours. The dried hyacinths were either ground (DWH) or heated in an incinerator at 600°C for 5 minutes to produce calcined water hyacinth (CWH).

2.2 Preparation of adsorbates

MB was bought from Merck and used as-is. Stock solutions were made in distilled water, and all study solutions were prepared by dissolving MB in distilled water.

2.3 Characterization of adsorbents

Adsorbent structures were examined using a JEOL-JSM5410LV scanning electron microscope. N2 adsorption-desorption measured BET surface area, pore size distribution, and volume. FTIR confirmed organofunctional groups on the

adsorbents' surface. pH_{PZC} was determined using the solid addition method [7-8].

2.4 Batch equilibrium studies

Water hyacinth powder was mixed with MB solutions in conical flasks, and stirred in a rotary shaker (25°C, 200 rpm) until equilibrium was reached. The diameters of DWH and CWH were controlled at approximately 2 mm and 0.02 mm, respectively. Centrifugation separated the mixture. MB residual levels were measured by a Shimadzu double-beam UV-visible spectrophotometer (668 nm. Batch equilibrium tests studied MB adsorption onto water hyacinth based on MB initial concentration, contact time, pH, and temperature. The adsorption capacity of the adsorbent is determined from the mass balance equation. It can be expressed as Eq. (1)

$$q_e = \frac{(C_0 - C_e)}{M} \times V \quad (1)$$

Where q_e *represents* the adsorption capacity (mg/g), C_0 is the initial concentration of the adsorbate (mg/L), Ce is the equilibrium concentration of the adsorbate, V is the volume of the solution (liters), and M is the mass of the adsorbent (gams). To understand the mechanism, we analyzed data using five mathematical isotherm models. These models were used to model the adsorption of MB onto adsorbents prepared from water hyacinth. The linear form of the Langmuir isotherm [14] can be described as Eq. (2):

$$\frac{1}{q_e} = \frac{1}{q_m} + \frac{1}{k_L q_m C_e} \quad (2)$$

where q_m is the maximum adsorption capacity (mg/g), and k_L is the Langmuir constant. The dimensionless separation factor R_L, which is used to predict the favorability of an adsorption system, can be described as Eq. (3):

$$R_L = \frac{1}{1 + K_L C_o} \quad (3)$$

where C_0 is the initial concentration of pharmaceuticals (mg/l).

The Freundlich isotherm in its linear form can be represented by Equation (4) as described in reference [15].

$$\ln q_e = \ln k_F + \frac{1}{n} \ln C_e \quad (4)$$

Where k_F is the Freundlich constant and n is the adsorption intensity (dimensionless).

The Dubinin-Radushkevich isotherm can be described by Eqs. (5) and (6) in linear form [15-16].

$$\ln q_e = \ln q_m - B\varepsilon^2 \quad (5)$$

$$\varepsilon = RT \ln\left(1 + \frac{1}{C_e}\right) \quad (6)$$

Where q_m is the maximum amount of adsorbate that can be adsorbed per unit mass of adsorbent, B is a constant related to the free energy of sorption per mole of adsorbate (J/mol), ε is the Polanyi potential and R is the gas constant (8.314 J/mol/K).

The linear form of the Temkin isotherm [15] can be described as Eq. (7):

$$q_e = \frac{RT}{b_T} \ln A_T + \frac{R_T}{b_T} \ln C_e \quad (7)$$

Where A_T (L/g) and b_T (J/mol) are the Temkin constants.

The Linear isotherm [16] can be described as Eq. (8):

$$q_e = K_p C_e \quad (8)$$

where K_p is the linear constant (liters/grams).

2.4.1 Studies on the effect of initial dye concentration

To test the effects of MB concentration on its adsorption onto water hyacinth, four different MB solutions were used (50, 100, 150, and 200 mg/L). Each solution was placed in a 250 mL Erlenmeyer flask with pH adjusted to 7 using a 0.01 M phosphate buffer. A fixed ratio of 2 g/L of water hyacinth to MB solution was maintained throughout the experiment.

2.4.2 Studies on the effects of pH

The impact of solution pH on the adsorption process was examined by altering the initial pH of the solution within the range from 2 to 10. The pH was adjusted using 0.1 M HCl and/or 0.1 M NaOH. The initial concentration of MB was fixed at 100 mg/L. The ratio of water hyacinth to MB solution was fixed at two g/L.

2.4.3 Batch Kinetic Studies

The procedure of batch kinetic studies was identical to that of the batch equilibrium studies. The aqueous samples were collected at preset time intervals, and the concentrations of MB were

measured correspondingly. The concentration of MB was reduced to 100 mg/L, and the pH of the solution was controlled at 7 with the help of a 0.01 M phosphate buffer. The ratio of water hyacinth to MB solution was maintained at two g/L. The mixtures were agitated in a rotary shaker at 25°C, 150 rpm. To evaluate the adsorption kinetics, MB concentrations were measured at different time intervals. The liquid from the adsorption mixture was separated through centrifugation, and the concentrations of residual MB in the supernatant were measured. Sampling and measurements were conducted until the MB solution reached equilibrium.

2.5 Column adsorption studies

Experimental studies were conducted to investigate the adsorption of MB solutions using groundwater hyacinth in a Pyrex glass column with an inner diameter of 25.4mm, and a height of 30cm. A known amount of groundwater hyacinth was packed into the column, and 5mm sized glass beads were used to ensure uniform flow of the solution. The effects of various column parameters on MB adsorption were investigated.

2.5.1 Studies on the effect of flow rate

The flow rate varied between 5, 10, and 15 ml/min. Inlet MB concentration was held constant at 100 mg/l.

2.5.2 Studies on the effect of inlet dye concentration

Inlet MB concentration was varied between 50, 100, and 150 mg/L. The flow rate was held constant at 10 mL/min.

3. Results and discussion

3. 1 Physico- chemical characteristics of the adsorbents

Table 1 displays the properties of the adsorbents. The nitrogen gas adsorption- desorption isotherms plots are shown in Figure 1.

CWH exhibited type IV isotherms, indicating that it is a mesoporous adsorbent, while DWH couldn't be classified. The average pore size of CWH was larger (81.89 Å) compared to DWH (26.65 Å). The specific surface area of CWH was higher (28.9 m2/g) than DWH (14.64 m^2/g). The pore volume of CWH was also higher (0.1186 cm3/g) than DWH (0.0274 cm^3/g). Calcination increased the pore size, specific surface area, and pore volume of water hyacinth. The pH_{PZC} for DWH was about 6.4, whereas for CWH, it was approximately 10.5. Approximately 95% of dried samples yield, while only 25% of calcined samples yield.

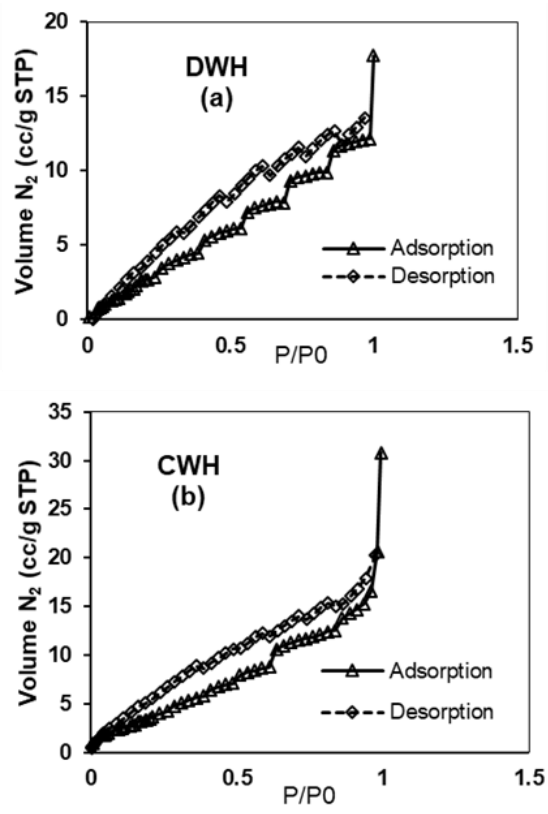

Figure1 Nitrogen gas adsorption- desorption isotherms of (a) DWH and (b) CWH.

Table 1. Physicochemical characteristics of DMH and CMH.

Adsorbents	Pore diameter (Å) [a]	BET surface area (m^2/g)[a]	Pore volume (cm^3/g) [a]	pH_{PZC}[b]
DWH	26.6	14.64	0.0274	6.4
CWH	81.89	28.90	0.1186	10.5

[a] determined by BET analysis of N_2 adsorption-desorption

[b] pH of net zero charge

The FTIR spectrum of DWH is compared with CWH, and this is shown in Figure 2. With DWH, peaks were found at 1318.1 cm^{-1}, 1371 cm^{-1},1384.6 cm^{-1}, 1421.3 cm^{-1}, 1622 cm^{-1}, 1734 cm^{-1}, 2292.6 cm^{-1}, 2925 cm^{-1}, and 3366 cm^{-1}. A peak at 1318.1 cm^{-1} indicates the presence of CH [7], and at 1371 cm^{-1}, the presence of CH_2 [40]. Peaks at 1384.6 cm^{-1} and

1421.3 cm^{-1} indicate the presence of OH phenolic and C-O of cellulose, respectively [9]. The presence of hemicellulose was seen at a peak of 1622 cm^{-1} [10]. Peaks observed at a 1734 cm^{-1} indicate the presence of acetyl and ester in the carboxyl group chain of the acid p-koumeril, as well as indicating the presence of lignin and hemicellulose [10]. This result agrees with previous work Thiripura and Ramesh presented [11]. Peaks observed at 2292.6 cm^{-1}, 2854-2952 cm^{-1}, and 3366-3400 cm^{-1} indicate the presence of CH_2, CH, and OH respectively [8-9]. In CWH, FTIR spectrum findings were different. Peaks at 1318.1 cm^{-1}, 1384.6 cm^{-1}, 1421.3 cm^{-1}, and 2292.6 cm^{-1} indicated the presence of CH, CH2, OH phenolic, and C-O of cellulose, which were found in DWH, but were not observed in CWH. The four peaks disappeared. They were broadened and fused together. The peak at 1622 cm^{-1} indicated the presence of hemicellulose, and the peak at 1734 cm^{-1} indicated the presence of acetyl and ester in the carboxyl group chain, as well as the presence of lignin and hemicellulose which also disappeared. The peak at 2292.6 cm^{-1}, indicated the presence of CH2 that still existed, and its peak was a little bit higher than in DWH. The peaks at 2854-2926 cm^{-1}, indicated the presence of CH, while the peaks at 3366-3400 cm^{-1} indicated the presence of OH; disappeared and became a linear plot. We analyzed the FTIR spectrum of DWH both before and after the adsorption of MB. Before adsorption, peaks were found at 1318.1 cm^{-1}, 1371 cm^{-1}, 1384.6 cm^{-1}, 1421.3 cm^{-1}, 1622 cm^{-1}, 1734 cm^{-1}, 2292.6 cm^{-1}, 2925 cm^{-1}, and 3366 cm^{-1}. After MB adsorption, new peaks were observed at 1593 cm^{-1}, 1714 cm^{-1}, and 1170 cm^{-1}. The peak at 1593 cm^{-1} was attributed to the C=N and C=C vibrations of MB [12]. The peak at 1714 cm^{-1} was assigned to the $C_{het} = N^{+}(CH_3)_2$ stretching vibrations of MB. A peak of 1170 cm^{-1} was attributed to the presence of MB [13]. The FTIR spectrum of CWH was analyzed before and after the adsorption of MB. Before adsorption, there was a peak at 2319.95 cm^{-1}, indicating the presence of N-H, and a peak at 2119.39 cm^{-1}, indicating the presence of C=C. Peaks which were found in DWH at 1318.1 cm^{-1}, 1384.6 cm^{-1}, 1421.3 cm^{-1}, 2292.6 cm^{-1}, 1622 cm^{-1}, 1734 cm^{-1}, 2854-2926 cm^{-1}, and 3366-3400 cm^{-1} disappeared. The peak at 2292.6 cm^{-1} indicated that the presence of CH_2 still existed, and its peak was slightly higher than in the DWH. After MB adsorption, new peaks were found at 1390 cm^{-1} and 1170 cm^{-1}. The peak at 1390 cm^{-1} is attributed to the symmetrical and asymmetrical bending vibrations of the CH_3 functional groups of MB [12]. The peak at 1170 cm^{-1} was attributed to the presence of MB [13]. The study results indicated that MB was adsorbed onto DWH and CWH.

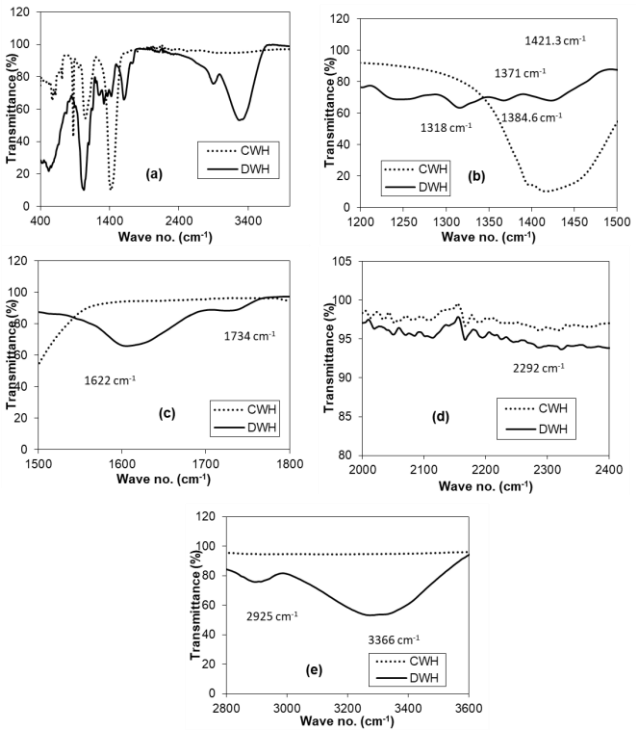

Figure 2 Fourier transform infrared spectroscopy (FT-IR) spectra of DWH and CWH.

Figures 3 and 4 display EDX-SEM images of DWH and CWH surfaces, morphologies, and their energy-dispersive X-Ray spectrum.

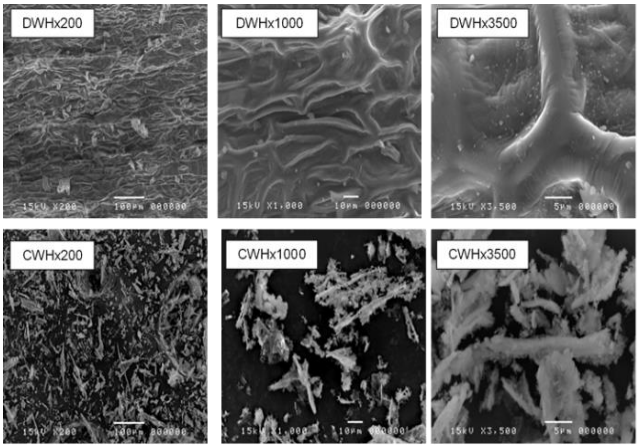

Figure 3 SEM images of DWH and CWH.

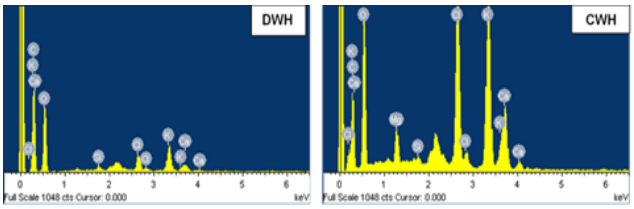

Figure 4 The energy dispersive X-ray spectrum of DWH and CWH.

SEM was used to examine the adsorbents at 200, 1000, and 3500 magnifications. DWH consisted of large particle agglomerates, while CWH consisted of smaller particle aggregates with variable shapes. The morphology of CWH was similar to heat- activated carbon. EDX revealed that DWH contained six elements, while CWH contained seven, including Mg.

3.2 Adsorption isotherm (Effect of initial dye concentration)

Figure5 shows MB adsorption onto water hyacinth at various initial concentrations.

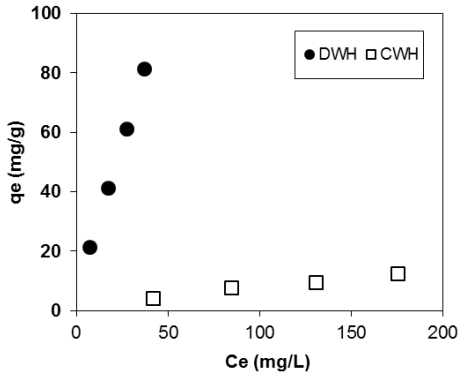

Figure 5 Adsorption capacity of DWH and CWH for MB.

DWH showed higher adsorption capacity than CWH for all MB concentrations. Adsorption capacity was higher at high MB concentration than at low MB concentration. This result agrees with previous research by Mridusmita Goswami [4]. A high initial dye concentration increases adsorption capacity by increasing the contact area and overcoming resistance to mass transfer. To understand the mechanism, we analyzed data using five mathematical isotherm models. These models were used to model the adsorption of MB onto adsorbents prepared from water hyacinth. The study found that the Langmuir isotherm model was the best fit for both DWH and CWH, as indicated by the calculated parameters and correlation coefficients (R^2). The MB adsorption isotherm data for MB adsorption onto various adsorbents, including water hyacinth, in this study, fitted with the Langmuir isotherm model [17]. The sorption of MB on WH was found to follow a Langmuir isotherm, suggesting a monolayer sorption on homogeneous energetic; active sites on the surface of the adsorbent. The maximum adsorption capacity (q_m) of the adsorbent prepared from the dried shoot of water hyacinth for MB in this study was 156.25 mg/g. It was higher than the q_m in the previous research done by Murai and Uma [18] (q_m= 17.58-46.35 mg/g). Compared with the adsorption capacity of the adsorbent prepared from dried root of water hyacinth, it was found that q_m for dried shoot in this study was lower than q_m for dried root in Syed Hadi Hasan's study [19] (q_m= 187.00 mg/g**),** but higher than in Soni et al., study [20] (q_m= 8.04 mg/g).

The adsorbents made from water hyacinth in this research had an adsorption capacity for MB of 156.25 mg/g, which is similar to picacarb granular activated carbon (160 mg/g) [4]. It had a higher adsorption capacity than Ephedra strobilaccea char (ESC) (31.1 mg/g) [21], phosphoric acid modified ESC (21.9 mg/g) [21], zinc chloride modified ESC (37.0 mg/g) [53], and cotton stalk (147 mg/g) [8]. However, its adsorption capacity for MB was lower than that of activated carbon from mature tea leaves (446.4 mg/g) [4], sulfonic acid modified activated carbon (714.3 mg/g) [4], sulfuric acid treated cotton stalk (555.5 mg/g) [22], and phosphoric acid treated cotton stalk (222.2 mg/g) [29]. Adsorbents other than activated carbon and sulfonic acid- modified activated carbon that had adsorption capacity for MB higher than water hyacinth were Filtrasorb400 (q_m= 255 mg/g), Fe_3O_4graphene@mesoporous SiO_2 nanocomposite (q_m= 178.4 mg/g) [22] and CuS nanoparticle (q_m= 208.3 mg/g) [23]. Due to its impressive adsorption capacity, water hyacinth adsorbent is a cost- effective and easily available alternative for removing cationic dye like MB. It has a similar adsorption capacity as picacarb granular activated carbon, it is higher than Ephedra strobilaccea char, but lower than expensive adsorbents.

3.3 Effects of pH

The results of the study are shown in Figure 6. The study found that the adsorption capacity of DWH increased as the pH level became more

neutral or basic (pH 7-9), whereas the adsorption capacity of CWH increased as the pH level became more acidic (pH 3-5). The adsorption capacity of DWH was lowest at pH 3, and that of CWH was lowest at pH 8 and 9. These findings are in agreement with the findings in other literature reports using various adsorbents to adsorb MB [23,24]. The pH-dependent surface charge of the adsorbent and the adsorbate can explain the reason for the observed phenomenon. For the case of DWH, the pH at which the surface charge is zero (pH_{PZC}) is found to be 6.4. When the pH of the solution is in the range of 5-7, the surface of DWH becomes positively charged, which is the same as the charge of MB. This results in a decreased adsorption capacity due to the repulsion of electric charges. However, when the pH of the solution is higher than 6.4, the surface of DWH becomes negatively charged, which is opposite to the charge of MB. This results in an increased adsorption capacity due to the attraction of electric charges.

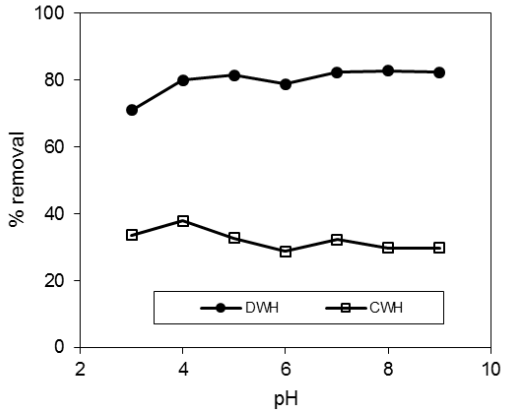

Figure 6 Effect of pH on MB adsorption by DWH and CWH.

Similarly, for CWH, the pH_{PZC} value is found to be 10.5. When the pH of the solution is greater than the pKa value of MB (which is equal to 3.8), both the surface of CWH and the MB molecules become positively charged, resulting in a repulsive force between them. This leads to a decreased adsorption capacity. On the other hand, when the pH of the solution is less than 3.8, the MB molecules become negatively charged, which is opposite to the charge on the surface of CWH. This results in an attractive force between them, leading to an increased adsorption capacity.

At low pH levels, excess H+ ions compete with MB for adsorption sites. As pH increases, negatively charged sites become more favorable for adsorption due to electrostatic attraction.

3.4 Adsorption kinetics

Figure 7 shows that the concentration of MB in the solution dropped quickly in the first 30 minutes for both adsorbents. After that, the concentration

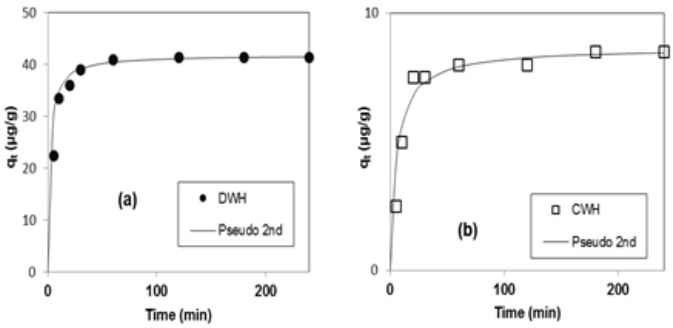

continued to decrease until it reached equilibrium in approximately 3 hours.

Figure 7 Adsorption kinetics of MB adsorbed by (a) DWH and (b) CWH.

3.4.1. Adsorption kinetic models

To evaluate the efficiency of the adsorption process, the experimental data was interpreted using the pseudo-first-order, pseudo-second-order, and Ritchie kinetic models. The pseudo-first-order kinetic model, as defined in Eq. (9) [25], can be expressed as follows:

$$\frac{1}{q_t} = \frac{k_1}{q_e t} + \frac{1}{q_e} \quad (9)$$

The amount of adsorbate adsorbed at equilibrium q_e and at a specific time, q_t is measured in milligrams per gram. The pseudo-first-order rate constant k_1 is also calculated in terms of per minute. The values of q_e and k_1 are derived from the slope and intercept of the plots of $1/q_t$ versus $1/t$, respectively.

The pseudo-second-order equation [25] can be defined as in Eq. (10):

$$\frac{t}{q_t} = \frac{1}{k_2 q_e^2} + \frac{t}{q_e} \quad (10)$$

Where k_2 is the pseudo- second- order rate constant, which is determined from the plots of t/q_t versus t. Furthermore, the initial adsorption rate (h) that is obtained from this model can be expressed as in Eq. (11):

$$h=k_2 q_e^2 \quad (11)$$

The Ritchie kinetic model [26] can be expressed as in Eq. (12)

$$\frac{1}{q_t}=\frac{1}{k_r q_e t}+\frac{1}{q_e} \quad (12)$$

where k_r is the Ritchie rate constant and is derived from the plots of $1/q_t$ versus $1/t$.

The adsorption parameters and kinetic models are calculated for MB adsorption on each adsorbent, as shown in Table 2. The correlation coefficients suggest that pseudo- second- order kinetics represent the adsorption of MB onto DWH and CWH. These findings are consistent with previous studies [27]. It is assumed that chemisorption is involved in the adsorption process. The adsorption rate was 24.5 mg/g/min in DWH and 1.54 mg/g/min in CWH. In Khan's study, 85% of MB was removed in 10-15 min. Reduction in the removal rate suggests monolayer coverage on the outer surface of adsorbent and pore diffusion on the inner surface through continuous agitation [17].

Table 2. Kinetic parameters for the biosorption of Methylene blue onto DWH and CWH.

Adsorbents	$q_{e,exp}$ (mg/g)	Pseudo-first order			Pseudo-second order			Ritchie			
		k_1 (L/min)	$q_{e,cal}$ (mg/g)	R^2	k_2 (g/mg/min)	$q_{e,cal}$ (mg/g)	R^2	h (mg/g/min)	k_r (L/min)	$q_{e,cal}$ (mg/g)	R^2
DWH	43.02	0.0086	9.972	0.579	0.0117	41.84	0.999	20.45	0.235	43.29	0.960
CWH	9.21	0.0081	3.317	0.677	0.0201	8.650	0.999	1.545	13.36	0.739	0.940

3.4.2 Intraparticle diffusion

The Boyd kinetic models were used to analyze the adsorption process, determining the diffusion mechanism and rate-limiting step. In solid-liquid adsorption, there are three steps: film diffusion, pore diffusion, and adsorption. The slowest step of the process limits the rate of adsorption. The Boyd kinetic model is a useful tool for analyzing these diffusion mechanisms [28]. The Boyd kinetic model can be expressed as Eqs. (13-16):

$$F=\frac{6}{\pi^2}\exp(-B_t) \quad (13)$$

$$F=\frac{q_t}{q_e} \quad (14)$$

$$Bt=-0.4977-\ln(1-F) \quad (15)$$

At any given time, the fraction of MB adsorbed can be denoted by F in comparison to the equilibrium point. B represents the Boyd kinetic coefficient, while D_i is the diffusion coefficient in m^2/g. Additionally, the radius of the adsorbent particles is represented by r. You can calculate the effective diffusion coefficient of solute in the adsorbent phase (D_i in m^2/g) by using the values of B and the relationship described in the references [29].

$$B=\frac{\pi^2 D_i}{r^2} \quad (16)$$

The data analyzed by Boyd kinetic models showed that the D_i of DWH was 6.8×10^{-9} m^2/g and the D_i of CWH was 7.3×10^{-13} m^2/g. DWH had much better adsorption for MB than CWH. Boyd equation was used to identify the rate- limiting step in adsorption. Boyd plots did not pass through the origin for both dried and CWH, indicating film diffusion as the rate-limiting step. This process was not controlled by pore diffusion, which is why CWH had inferior adsorption for MB compared to DWH.

3.5 Column studies

Water hyacinth adsorbent in the column removed MB in the mass transfer zone of the breakthrough curves. At first, high removal was observed, which gradually decreased until a breakthrough was established. Breakthrough curves were obtained by plotting effluent concentration against service time. Treated volume was used to calculate treated effluent volume.

$$V_t=Qt_e \quad (17)$$

Where Q is the volumetric flow rate (mL/min), and t_e is the time at exhaustion (min).

The maximum column capacity (q_{total},(mg)), for a given concentration of feed and flow rate, is a measure of the area under the plot of the concentration of MB adsorbed ($C_{ad}=C_0-C_t$). This can be expressed as C_{ad} (mg/L) against affluent time t (min) and is obtained from Eq. (18) [30]:

$$q_{total}=\frac{Q}{1000}\int_{t=0}^{t=t_{total}} C_{ad}dt \quad (18)$$

Where q_{total}, Q, and C_{ad} are the total flow time (min), volumetric flow rate (mL/min), and concentration of MB adsorbed (mg/L) respectively. Equilibrium uptake ($q_{eq(exp)}$) (mg/g) is calculated as:

$$q_{eq(exp)}=\frac{q_{total}}{m} \quad (19)$$

The variable m represents the total amount of adsorbent (in grams) used in the column.

3.5.1 Effect of flow rate

The breakthrough curves for the effect of solution flow rates on the adsorption process are shown in Fig. 8.

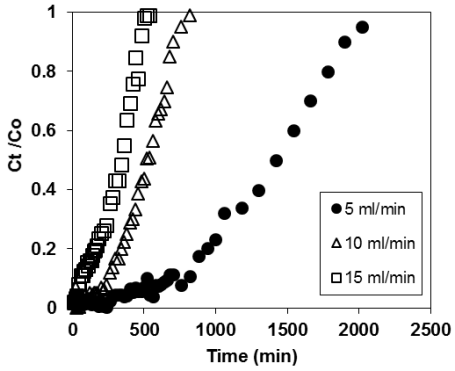

Figure 8 Breakthrough curves for MB adsorption by DWH at different flow rates.

The experiment tested the effect of varying flow rates on methylene blue adsorption at a fixed 100mg/L concentration. Higher flow rates led to faster breakthrough points due to an increased mass transfer. At 5 mL/min, the adsorption capacity was 127.89 mg/g, but at 10 and 15 mL/min, it decreased to 115.61 mg/g and 72.24 mg/g, respectively. Higher flow rates caused a decrease in breakthrough time and adsorption capacity. Table 3 shows the column data parameters at different flow rates.

Table 3. Column data parameters were obtained at different flow rates and influent concentrations.

Flow rate (mL/min)	Influent concentration (mg/L)	q_{total} (mg)	$q_{eq(exp)}$ (mg/g)
5	100	639.46	127.89
10	100	578.05	115.61
15	100	361.22	72.24
10	50	475.14	95.03
10	150	601.95	120.39

3.5.2 Effect of inlet MB concentrations

We studied the effect of different inlet concentrations of MB (50 mg/L, 100 mg/L, and 150 mg/L) on fixed-bed column adsorption of MB by the water hyacinth plant at a constant flow rate of 10mL/min. Results showed that a lower concentration of 50mg/L resulted in extended breakthrough time and a greater volume of polluted water treated. However, a higher concentration of 150mg/L resulted in a shorter breakthrough time and only a small volume of treated wastewater. The adsorption capacity increased as the influent concentration increased. The adsorption capacities were 95.03 mg/g, 115.61 mg/g, and 120.39 mg/g for 50 mg/L, 100 mg/L, and 150 mg/L respectively, and this is in agreement with previous studies. Results suggest that water hyacinth is effective in removing MB from wastewater.

Figure 9 Breakthrough curves for MB adsorption

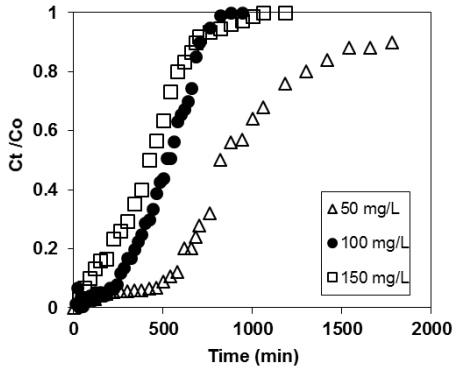

by DWH at different initial concentrations.

3.5.3 The breakthrough curves modeling

Various models are used to predict MB breakthrough in fixed bed columns. The Thomas model is one such model which can be used to calculate the adsorption rate constant. The model assumes that adsorption is limited by mass transfer and does not involve axial dispersion. Thomas's model can be described as:

$$\frac{C_t}{C_o}=\frac{1}{1+e^{\left[(q_0 m-C_0 vt)\frac{k_{th}}{v}\right]}} \quad (20)$$

Where k_{th} is the Thomas rate constant (mL/min/mg), q_0 is the equilibrium adsorption capacity (mg/g). m is the mass of the adsorbent, C_0 and C_t are the concentration of MB in the

effluent and at time t (mg/L), and v is the flow rate (mL/min).

The Yoon-Nelson model assumes that the rate of decrease in the adsorption probability for each adsorbate molecule depends on the probability of adsorbate adsorption and the probability of an adsorbate breakthrough on the adsorbent [31]. The model can be expressed by Eq.(21)

The Yoon Nelson model can be expressed by Eq. (21)

$$\frac{C_t}{C_o}=\frac{1}{1+e^{[-k_{YN}(t-T)]}} \quad (21)$$

Where k_{YN} is the Yoon-Nelson rate constant (1/min), while T is the time required to reach 50% adsorbate breakthrough (min).

The Modified-dose-response model equation is expressed as:

$$\frac{C_t}{C_o}=1-\frac{1}{1+\left(\frac{vt}{b}\right)^a} \quad (22)$$

Where a and b are both the constant of the modified-dose-response model.

The Adam' s- Bohart model [32] can be expressed by Eq. (23)

$$\ln\frac{C_t}{C_o}=k_{AB}C_o t-k_{AB}N_o\frac{Z}{F} \quad (23)$$

Where k_{AB} represents the Adam' s- Bohart kinetic rate constant ($L/mg/min$), F is the linear velocity calculated by dividing the flow rate by the column section area, Z is the bed depth of the column, and N_o is the saturation concentration.

The data from both DWH and CWH matched well with Thomas' model as well as Yoon Nelson's model. The correlation coefficient values between the experimental and predicted values using the Thomas model and the Yoon Nelson model ranged from 0.9011 to 0.9962. It indicated that the MB adsorption mechanism by DWH and CWH was a Langmuir type of sorption, and followed pseudo second order kinetics monolayer chemical sorption [42].

4. Conclusions

Two adsorbents, DWH and CWH, were developed to adsorb MB. DWH had smaller porosity, but a higher adsorption capacity than CWH. Both adsorbents showed the presence of MB after adsorption. DWH had a pH_{PZC} of 6.4, and CWH had a pH_{PZC} of 10.5. DWH is a good alternative for removing cationic dyes due to its high abundance and low cost. The adsorption isotherm data resembled that of the Langmuir model. In the kinetic study, the adsorption followed pseudo-second-order kinetics. In the column study, breakthrough points were observed to occur faster at higher flow rates. The data from both DWH and CWH matched up well with both Thomas and Yoon Nelson models.

6. Acknowledgment

The authors would like to acknowledge the financial support from the National Research Council of Thailand (NRCT) (fiscal year 2018) and Rajamangala University of Technology Lanna, Thailand

7. References

[1] Al-Ghouti MA, Khraisheh MA, Ahmad MN, Allen S. Adsorption behaviour of methylene blue onto Jordanian diatomite: a kinetic study. J Hazard Mater. 2009;165(1-3):589-98.

[2] Al-Ghouti MA, Al-Degs YS, Khraisheh MA, Ahmad MN, Allen SJ. Mechanisms and chemistry of dye adsorption on manganese oxides-modified diatomite. J Environ Manage. 2009;90(11):3520-7.

[3] El Qada EN, Allen SJ, Walker GM. Influence of preparation conditions on the characteristics of activated carbons produced in laboratory and pilot scale systems. Chem Eng J. 2008;142(1):1-3.

[4] Goswami M, Phukan P. Enhanced adsorption of cationic dyes using sulfonic acid modified activated carbon. J Environ Chem Eng. 2017;5(4):3508-17.

[5] Albadarin AB, Mo J, Glocheux Y, Allen S, Walker G, Mangwandi C. Preliminary investigation of mixed adsorbents for the removal of copper and methylene blue from aqueous solutions. Chem Eng J. 2014;255:525-34.

[6] Iakovleva E, Sillanpää M, Maydannik P, Liu JT, Allen S, Albadarin AB, Mangwandi C. Manufacturing of novel low-cost adsorbent: Co-granulation of limestone and coffee waste. J Environ Manage. 2017;203:853-60.

[7] Ala'a H, Ibrahim KA, Albadarin AB, Ali-Khashman O, Walker GM, Ahmad MN. Remediation of phenol-contaminated water by adsorption using poly (methyl methacrylate) (PMMA). Chem Eng J. 2011;168(2):691-9.
[8] Ibrahim M, Kühn O, Scheytt T. Molecular spectroscopic study of water hyacinth dry matter. Open Chem Phys J. 2009;2(1).
[9] Ibrahim M, Osman O, Mahmoud AA, Elhaes H. Spectroscopic analyses of water hyacinth: FTIR and modeling approaches.
[10] Istirokhatun T, Rokhati N, Rachmawaty R, Meriyani M, Priyanto S, Susanto H. Cellulose isolation from tropical water hyacinth for membrane preparation. Procedia Environ Sci. 2015;23:274-81.
[11] Sundari MT, Ramesh A. Isolation and characterization of cellulose nanofibers from the aquatic weed water hyacinth Eichhornia crassipes. Carbohydr Polym. 2012;87(2):1701-5.
[12] Bartošová A, Blinová L, Sirotiak M, Michalíková A. Usage of FTIR-ATR as non-destructive analysis of selected toxic dyes. Res Pap Fac Mater Sci Technol Slovak Univ Technol. 2017;25(40):103-11.
[13] Pradhan AC, Paul A, Rao GR. Sol-gel-cum-hydrothermal synthesis of mesoporous Co-Fe@Al2O3−MCM-41 for methylene blue remediation. J Chem Sci. 2017;129:381-95.
[14] Langmuir I. The constitution and fundamental properties of solids and liquids. Part I. Solids. J Am Chem Soc. 1916;38(11):2221-95.
[15] Temkin MAP, V. Kinetics of Ammonia Synthesis on Promoted Iron Catalysts. Acta Physicochim URSS. 1940;12:217-22.
[16] Faust SD, Aly OM. Batch Systems and Fixed and Fluidized Beds. In: Adsorption Processes for Water Treatment. 1st ed. New York: Butterworth-Heinemann; 1986. p. 123-165.
[17] Khan MR, Mozumder SI, Islam A, Prasad DR, Alam MM. Methylene blue adsorption onto water hyacinth: batch and column study. Water Air Soil Pollut. 2012;223:2943-53.
[18] Murali K, Uma RN. Removal of basic dye (methylene blue) using low cost biosorbent: Water hyacinth. Int J Adv Engg Tech. 2016;VII(II):386-91.
[19] Hasan SH, Ranjan D, Talat M. Water hyacinth biomass (WHB) for the biosorption of hexavalent chromium: optimization of process parameters. BioResources. 2010;1.
[20] Soni M, Sharma AK, Srivastava JK, Yadav JS. Adsorptive removal of methylene blue dye from an aqueous solution using water hyacinth root powder as a low cost adsorbent. Int J Chem Sci Appl. 2012;3(3):338-45.
[21] Raposo F, De La Rubia MA, Borja R. Methylene blue number as useful indicator to evaluate the adsorptive capacity of granular activated carbon in batch mode: Influence of adsorbate/adsorbent mass ratio and particle size. J Hazard Mater. 2009; 165(1-3):291-9.
[22] Wu XL, Shi Y, Zhong S, Lin H, Chen JR. Facile synthesis of Fe3O4-graphene@mesoporous SiO2 nanocomposites for efficient removal of Methylene Blue. Appl Surf Sci. 2016; 378:80-6.
[23] Mazaheri H, Ghaedi M, Asfaram A, Hajati S. Performance of CuS nanoparticle loaded on activated carbon in the adsorption of methylene blue and bromophenol blue dyes in binary aqueous solutions: using ultrasound power and optimization by central composite design. J Mol Liq. 2016; 219:667-76.
[24] Qi C, Zhao L, Lin Y, Wu D. Graphene oxide/chitosan sponge as a novel filtering material for the removal of dye from water. J Colloid Interface Sci. 2018; 517:18-27.
[25] Ho YS, McKay G. Pseudo-second order model for sorption processes. Process Biochem. 1999; 34(5):451-65.
[26] Ritchie AG. Alternative to the Elovich equation for the kinetics of adsorption of gases on solids. J Chem Soc, Faraday Trans 1: Phys Chem Condens Phases. 1977; 73: 1650-3.
[27] Yu X, Wei C, Wu H. Effect of molecular structure on the adsorption behavior of cationic dyes onto natural vermiculite. Sep Purif Technol. 2015;156:489-95.

[28] Tong KS, Kassim MJ, Azraa A. Adsorption of copper ion from its aqueous solution by a novel biosorbent Uncaria gambir: Equilibrium, kinetics, and thermodynamic studies. Chem Eng J. 2011;170(1):145-53.
[29] Gautam RK, Chattopadhyaya MC. Kinetics and equilibrium isotherm modeling: Graphene-based nanomaterials for the removal of heavy metals from water. In: Nanomaterials for Wastewater Remediation. 2016. p. 79-109.
[30] Faust SD, Aly OM. Batch Systems and Fixed and Fluidized Beds. In: Adsorption Processes for Water Treatment. 1st ed. New York: Butterworth-Heinemann; 1986. p. 123-65.
[31] Yoon YH, Nelson JH. Application of gas adsorption kinetics I. A theoretical model for respirator cartridge service life. Am Ind Hyg Assoc J. 1984;45(8):509-16.
[32] Bohart GS, Adams EQ. Some aspects of the behavior of charcoal with respect to chlorine. J Am Chem Soc. 1920;42(3):523-44.
[33] Demarci CA, Debrassi A, Dal Magro J, Nedelko N, Ślawska-Waniewska A, Dłużewski P, et al. Adsorption of Cr (VI) on crosslinked chitosan–Fe (III) complex in fixed-bed systems. J Water Process Eng. 2015;7:141-52.